



HAL
open science

Spacecraft Outgassing Observed by the BepiColombo Ion Spectrometers

M. Fränz, M. Rojo, T. Cornet, L. Hadid, Y. Saito, N. André, A. Varsani, D. Schmid, H. Krüger, N. Krupp, et al.

► **To cite this version:**

M. Fränz, M. Rojo, T. Cornet, L. Hadid, Y. Saito, et al.. Spacecraft Outgassing Observed by the BepiColombo Ion Spectrometers. *Journal of Geophysical Research Space Physics*, 2024, 129 (1), 10.1029/2023JA032044 . hal-04465741

HAL Id: hal-04465741

<https://hal.science/hal-04465741>

Submitted on 21 Feb 2024

HAL is a multi-disciplinary open access archive for the deposit and dissemination of scientific research documents, whether they are published or not. The documents may come from teaching and research institutions in France or abroad, or from public or private research centers.

L'archive ouverte pluridisciplinaire **HAL**, est destinée au dépôt et à la diffusion de documents scientifiques de niveau recherche, publiés ou non, émanant des établissements d'enseignement et de recherche français ou étrangers, des laboratoires publics ou privés.



Distributed under a Creative Commons Attribution - NonCommercial - NoDerivatives 4.0 International License

JGR Space Physics




















RESEARCH ARTICLE

10.1029/2023JA032044

Spacecraft Outgassing Observed by the BepiColombo Ion Spectrometers

Key Points:

- Strong outgassing from the BepiColombo spacecraft was observed during first Mercury Flyby in 2021 and later during interplanetary cruise
- The gas composition is dominated by water molecules
- The ion energy spectra sometimes show a double band structure which we interpret as being caused by different ionization locations within a negative spacecraft potential

M. Fränz¹ , M. Rojo², T. Cornet³, L. Z. Hadid⁴, Y. Saito⁵ , N. André² , A. Varsani⁶ , D. Schmid⁶ , H. Krüger¹ , N. Krupp¹ , D. Delcourt⁴ , B. Katra⁴ , Y. Harada⁷ , S. Yokota⁸ , C. Verdeil² , S. Aizawa² , A. Millilo⁹ , S. Orsini⁹, V. Mangano⁹ , B. Fiethe¹⁰, J. Benkhoff¹¹ , and G. Murakami⁵ 

¹Max Planck Institute for Solar System Research, Göttingen, Germany, ²Institut de Recherche en Astrophysique et Planétologie, CNRS-UPS-CNES, Toulouse, France, ³Aurora Technology BV for ESA-European Space Agency, European Space Astronomy Centre (ESAC), Madrid, Spain, ⁴Laboratoire de Physique des Plasmas (LPP), CNRS, Observatoire de Paris, Ecole Polytechnique, Institut Polytechnique de Paris, Sorbonne Université, Université Paris Saclay, Palaiseau, France, ⁵ISAS-JAXA, Sagihamara, Japan, ⁶WFI, Graz, Austria, ⁷Kyoto University, Kyoto, Japan, ⁸Osaka University, Toyonaka, Japan, ⁹INAF-IAPS, Rome, Italy, ¹⁰IDA, TU Braunschweig, Braunschweig, Germany, ¹¹ESA-ESTEC, Noordwijk, The Netherlands

Correspondence to:

M. Fränz,
fraenz@mps.mpg.de

Citation:

Fränz, M., Rojo, M., Cornet, T., Hadid, L. Z., Saito, Y., André, N., et al. (2024). Spacecraft outgassing observed by the BepiColombo ion spectrometers. *Journal of Geophysical Research: Space Physics*, 129, e2023JA032044. <https://doi.org/10.1029/2023JA032044>

Received 1 SEP 2023
 Accepted 30 DEC 2023

Author Contributions:

Conceptualization: M. Fränz, H. Krüger, A. Millilo, V. Mangano
Data curation: M. Rojo, T. Cornet, Y. Saito, A. Varsani, D. Schmid, D. Delcourt, B. Katra, Y. Harada, S. Yokota, C. Verdeil, S. Aizawa, B. Fiethe
Formal analysis: M. Fränz
Funding acquisition: Y. Saito, N. André, N. Krupp, D. Delcourt, A. Millilo, S. Orsini, J. Benkhoff
Investigation: M. Fränz, L. Z. Hadid, N. André, A. Varsani, H. Krüger, D. Delcourt, Y. Harada, C. Verdeil, S. Orsini
Methodology: M. Fränz, H. Krüger, A. Millilo, V. Mangano
Project Administration: Y. Saito, N. André, A. Varsani, D. Schmid, H. Krüger, N. Krupp, D. Delcourt, A. Millilo, S. Orsini, J. Benkhoff, G. Murakami

Abstract During the first flyby of the BepiColombo composite spacecraft at Mercury in October 2021 ion spectrometers observed two intense spectral lines with energies between 10 and 70 eV. The spectral lines persisted also at larger distances from Mercury and were observed again at lower intensity during cruise phase in March 2022 and at the second and third Mercury flyby as a single band. The ion composition indicates that water is the dominant gas source. The outgassing causes the composite spacecraft to charge up to a negative potential of up to -50 V. The distribution and intensity of the lower energy signal depends on the intensity of low energy electron fluxes around the spacecraft which again depend on the magnetic field orientation. We interpret the observation as being caused by water outgassing from different source locations on the spacecraft being ionized in two different regions of the surrounding potential. The interpretation is confirmed by two dimensional particle-in-cell simulations.

Plain Language Summary The BepiColombo spacecraft is on its way through the inner solar system in a composite configuration consisting of two satellites and a propulsion unit with two large solar arrays. This configuration will only be separated after orbit insertion in December 2025. During the cruise phase and planetary flybys in the years 2021–2023 the ion spectrometers onboard the two satellites observed strong fluxes of low energy positive ions. We interpret these observations as being caused by outgassing of water from the spacecraft and a negative charging of the spacecraft caused by a high electron density surrounding the spacecraft. Around the first Mercury flyby in October 2021 all ion spectrometers observed two separate peaks in the low energy ion spectra. We explain these as being caused by water molecules being ionized by strong photon and electron fluxes in different regions of the negative potential surrounding the spacecraft. From these different potential regions ions are accelerated back to the spacecraft.

1. Introduction

The contamination of spacecraft instruments by outgassing of material from the interior of spacecraft has been known to be a problem since the beginning of the space age. Specifically during the time of the space shuttle the effects of outgassing and ionization of material have been investigated (Murad, 1985). Specific investigations were designed for the Midcourse Space Experiment and results reported in Green (2001). Strong outgassing of water was also observed on this mission (Uy et al., 2003). For spacecraft in interplanetary space much less was known about the intensity of outgassing until the neutral gas instrumentation of the Rosetta spacecraft allowed a comprehensive study by Schläppi et al. (2010) using data of the ROSINA neutral gas sensors. They reported an initial gas pressure of 10^{-8} mbar 10 days after launch and an exponential fall off with a time constant of 30 days afterward leading to a pressure of $3 \cdot 10^{-11}$ mbar 6 years after launch. The latter is corresponding to a water vapor density of $5 \cdot 10^5/\text{cm}^3$ at an assumed temperature of 150 K. The water group (H_2O , OH, O) fraction of the outgassing was around 90% most of times, though the fraction of fluorine (19 amu) was also significant, the rest being dominated by CO or N_2 (28 amu)—probably by fragmentation of larger molecules, H_2CO (30 amu) and CO_2 (44 amu). The operation of spacecraft thrusters also contributed to the deposition of water on the spacecraft. Also

© 2024 The Authors.

This is an open access article under the terms of the [Creative Commons Attribution-NonCommercial License](#), which permits use, distribution and reproduction in any medium, provided the original work is properly cited and is not used for commercial purposes.

Resources: M. Fränz, M. Rojo, T. Cornet, L. Z. Hadid, A. Varsani, D. Schmid
Software: M. Fränz, B. Fiethe
Validation: M. Fränz, M. Rojo, T. Cornet, L. Z. Hadid, A. Varsani, H. Krüger, D. Delcourt, Y. Harada, S. Aizawa, V. Mangano, B. Fiethe
Visualization: M. Fränz
Writing – original draft: M. Fränz
Writing – review & editing: M. Fränz, M. Rojo, T. Cornet, L. Z. Hadid, N. André, A. Varsani, H. Krüger, N. Krupp, Y. Harada, A. Millilo, V. Mangano

each spacecraft attitude maneuver caused temporal increases in outgassing by illuminating previously shadowed parts of the spacecraft. All observations by Rosetta were performed at solar distances between 1 and 2.5 AU.

Interestingly all observations of outgassing from spacecraft reported so far have been made either by estimating deposit layers on camera systems or by neutral gas instruments. A general review of the effect of water ice on spacecraft can be found in Euclid Collaboration et al. (2023). Specifically for Rosetta no observations of outgassing by the Rosetta plasma instruments have been reported (Nilsson et al., 2015). On the other hand several studies investigated the effect of high cometary gas densities on the spacecraft potential (Johansson et al., 2020, 2021; Odelstad et al., 2015, 2017). Odelstad et al. (2015) showed that neutral gas densities above $10^7/\text{cm}^3$ correlate with a negative charging of the spacecraft. The corresponding electron (and ion) densities were in this case higher than $30/\text{cm}^3$ (Johansson et al., 2021) and the negative potential showed a log dependence on plasma density above that threshold (Johansson et al., 2021). From these studies we may conclude that the ion density caused by the outgassing around the Rosetta spacecraft either never exceeded this threshold or the respective electron spectrum did not lead to a negative charging of the spacecraft. Otherwise positively charged water ions would have been observed by the ion spectrometer onboard Rosetta in cruise phase. This is also consistent with the observed outgassing density of less than $10^7/\text{cm}^3$ (except for the first 100 days of the mission) reported by Schläppi et al. (2010).

In this paper we report on observations of spacecraft outgassing by the BepiColombo spacecraft in cruise phase (Benkhoff et al., 2021). BepiColombo was launched in October 2018 and will be inserted into orbit around Mercury in December 2025. At the time of writing the spacecraft has performed one Earth, two Venus and three Mercury flybys and crossed the interplanetary space between 0.3 and 1 AU several times. During cruise phase the spacecraft is in a stacked configuration (see Figure 1) consisting of the JAXA/MMO satellite (later renamed to Mio, Murakami et al., 2020), located inside the MOSIF shield, the MPO satellite, and the MTM transfer module, all provided by ESA. In this stacked configuration only a limited number of scientific instruments are switched on and most of these can only operate in limited modes. Nevertheless scientific observations have been planned and partly executed during planetary flybys and in solar wind (Hadid et al., 2021; Mangano et al., 2021).

The surprising new fact about the outgassing observed by BepiColombo is that observations were made by the ion spectrometers measuring positive ions only. This would imply a negative charging of the spacecraft either by a very high electron density or by modified charging physics closer to the Sun. Negative spacecraft potentials were already observed for the Helios spacecraft between 0.3 and 1 AU, but determining a quantitative value from observations was difficult (Isensee & Maassberg, 1981). Voigt et al. (1981) inferred values up to -20 V by simulation. Later Ergun et al. (2010) also predicted negative potentials for the Solar Probe mission. These simulations were refined by Guillemant et al. (2012) predicting values up to -20 V at 0.04 AU. A recent analysis of the Solar Probe data (Diaz-Aguado et al., 2021) came to values around -13 V close to the Sun. Guillemant et al. (2013) give a general overview on potential simulations for spacecraft between 0.044 and 1 AU and describe the correlation between potential and electron mean free path (*Debye length*).

2. Instruments and Data

We use data obtained by the ion Mass Spectrum Analyzer(MSA) and Mercury Ion spectral Analyzer (MIA), the Mercury Electron Analyzers MEA1 and MEA2 belonging to the Mercury Plasma Particle Experiment (MPPE, Saito et al. (2021)) onboard the MMO (=Mio) spacecraft, and by the Planetary Ion Camera (PICAM) belonging to the Particle Instrument Suite for Determining the Sun-Mercury Interaction (SERENA, Orsini et al. (2021)) onboard the MPO spacecraft. Parameters of the different instruments are listed in Table 1. Due to the limited telemetry allocation for the MMO spacecraft a large amount of data gaps are encountered specifically for the larger data records. Acronyms are listed in Table 2 at the end of the paper. The location of all spectrometers is shown in Figure 1.

The MSA ion sensor (Delcourt et al., 2016) is a top-hat electrostatic analyzer with an energy range of $1 \text{ eV}/q$ to $38 \text{ keV}/q$ at 8% resolution. It has a field-of-view of $5^\circ \times 260^\circ$ but in the stacked configuration during cruise-phase this is restricted to about $5^\circ \times 33^\circ$ toward open space. After the energy filtering ions are pre-accelerated by 8 kV. This allows them to pass a carbon foil where secondary electrons cause a start signal on a start micro channel plate (MCP). Ions neutralized or charged negative by the foil passage create a stop signal at a stop MCP. Start and stop signal deliver a time-of-flight of the ion (TOF). Ions remaining positive may create a stop signal on the start MCP but the respective products are not transmitted in cruise phase. The mass range is 1–60 amu with a mass resolution $m/\Delta m = 10$ for the “TSTL” product (Saito et al., 2021) available in cruise phase. This product represents an

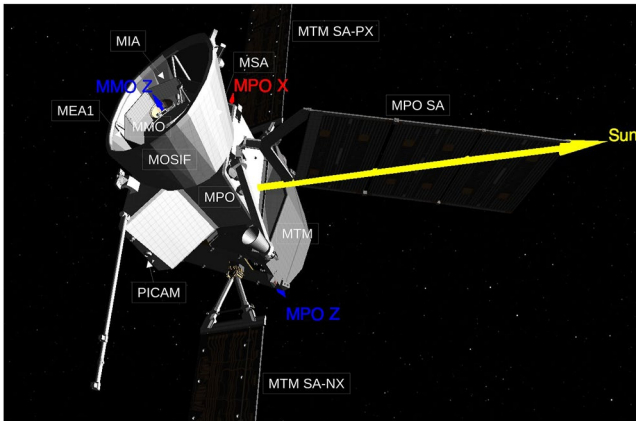


Figure 1. BepiColombo stacked configuration during Mercury flybys and cruise phase. Shown are the four units: MTM, MPO, MOSIF, and MMO with the solar arrays MTM SA-PX, MTM SA-NX, and MPO SA and the location of the spectrometers MIA, MSA, MEA1, and Planetary Ion Camera. The MPO coordinate frame is indicated by MPO X (red), MPO Z (=MMO -Z, blue) and solar direction (=MPO Y, yellow). The MMO satellite and its sensors is completely shadowed by the MOSIF shield (figure produced by Spice Cosmographia).

energy versus TOF matrix with resolution 64 energies \times 1024 TOF channels at time resolution of 256 s. Other products downlinked in cruise phase are energy spectra (64 energies) for protons (“M1L”), He⁺⁺ (“M2L”) and ions with $m/q \geq 4$ (“M3L”) at 66 s time resolution. Full operation of the onboard software started only with the second Venus flyby in August 2021.

The MIA ion sensor (Saito et al., 2021) uses also a top-hat electrostatic analyzer with energy resolution varying from 2.2% to 12.7%. The field of view is adjustable from $6.4^\circ \times 270^\circ$ – $9.6^\circ \times 270^\circ$ with respective geometric factors of 1.23×10^{-5} and 4.64×10^{-4} cm²-sr-eV/eV for the products used in this study. These are the omni-directional energy spectra (“Et”) which are divided into 4 sectors “d1” to “d4” with 128 energy steps in solar wind mode at time resolution of 16 s. In magnetospheric mode 32 energy steps with 4 s time resolution is used.

The MEA electron sensors (Saito et al., 2021) use also a top-hat electrostatic analyzer with energy resolution of 10%. Their field of view is $8^\circ \times 360^\circ$ but also limited in the stacked configuration. In this study we use only omni-directional energy spectra (“Et-OMN”) with 16 energy steps and 4s time resolution available in low telemetry mode.

The SERENA-PICAM sensor (Orsini et al., 2021) is an ion-camera using electro-static mirrors with 15% energy resolution. It has a field of view 1.5π at a resolution of $20^\circ \times 60^\circ$. In addition it has the capability to measure the TOF of ions using an electro-static shutter. In this study we only use omni-directional energy spectra at 32 s time resolution from the imaging mode (IMG) of the sensor.

In addition we use magnetic field data obtained by the MMO-MGF instrument (Baumjohann et al., 2020) down-sampled to 4 s time resolution and temperature and voltage data recorded by several platform house keeping sensors mounted on MMO, MPO, MTM, and the solar arrays—usually down-sampled to 1 min resolution. We should note that all instruments have been designed for operation after separation of the BepiColombo stack and not for operation in cruise phase. This means that calibration of data products are still very preliminary.

3. Initial Observation at First Mercury Flyby

During the first and second Venus flybys the ion spectrometers MIA and MSA onboard BepiColombo already recorded an increased intensity of low energy ions. But since during these flybys no synchronous observations at low energies of all different sensors were possible it was not clear whether the observations showed an instrumental effect or not. Only during the first Mercury Flyby on 1 October 2021, it became obvious that the low energy signal was observed by all three ion spectrometers. Figure 2 shows the low energy ion energy spectra observed by the MIA and MSA sensors for 2 days around the first Mercury flyby. Figure 3 shows a close-up around closest approach (CA, 10 January 2021 23:40 UTC) with the additional spectra observed by SERENA-PICAM and MEA-1. A general overview of observations by PICAM during the flyby is given in Orsini et al. (2022). Figure 4 shows the geometry of the flyby with the orientation of the stacked BepiColombo spacecraft axes. Over-plotted

Table 1
Instruments Onboard BepiColombo and Properties Used in This Study

| Acronym units | Type | Energy range (eV/q) | Mass res. (m/ Δ m) | Geometric factor (cm ² -sr-eV/eV) | Field of view (deg) |
|---------------|--------------|---------------------|---------------------------|--|------------------------------|
| MSA | Ion mass | 1–38 k | 10 | 3.6×10^{-4} | $5^\circ \times 33^\circ$ |
| MIA | Ion | 12–26 k | n.a. | 4.64×10^{-4} | $9.6^\circ \times 270^\circ$ |
| PICAM | Ion mass | 10–3.0 k | (10) | 4.9×10^{-5} | $20^\circ \times 60^\circ$ |
| MEA1 | Electron | 3–25.5 k | n.a. | 6.7×10^{-5} | $8^\circ \times 360^\circ$ |
| MEA2 | Electron | 3–25.5 k | n.a. | 4.0×10^{-6} | $8^\circ \times 360^\circ$ |
| MGF | Magnetometer | | | | |

Table 2
List of Technical Abbreviations

| Acronym | Name |
|----------|--|
| IMG | PICAM image mode data |
| MCP | Micro Channel Plate |
| MEA | Mercury Electron Analyzers |
| MFB1,2,3 | First, Second, Third Mercury Flyby |
| MGF | Mercury Flux Gate magnetometer |
| MIA | Mercury Ion spectral Analyzer |
| MMO | (=Mio) Mercury Magnetospheric Orbiter |
| MOSIF | MMO sunshield and Interface Structure |
| MPO | Mercury Planetary Orbiter |
| MPPE | Mercury Plasma Particle Experiment |
| MSA | Mass Spectrum Analyzer |
| MTM | Mercury Transfer Module |
| MIL | M2L, M3L Mass spectral products for protons, He ⁺⁺ , heavy ions |
| PIC | Particle in Cell simulation |
| PICAM | Planetary Ion Camera |
| SA-PX | Solar Array Positive X-axis |
| SA-NX | Solar Array Negative X-axis |
| SERENA | Search for Exospheric Refilling and Emitted Natural Abundances |
| TOF | Time-of-Flight |
| TSTL | Time-of-flight Stop Low telemetry product |
| VFB1,2 | First, Second Venus Flyby |

along the track is the total low energy ion flux observed by MIA. It shows that the solar illumination of the spacecraft does not change significantly around the CA. A rotation of the spacecraft only happened before and after this period shown by the orientation of the spacecraft Z-axis in Figure 2.

We note first, that the low energy signal was observed for a long time before and after the flyby at distances from Mercury of more than 100 Mercury radii (R_M , Figure 2). This means that it is not caused by the proximity of Mercury. The highest intensity was observed about 20 min after the CA at a time when also the temperature of the MMO side panel and of the MOSIF shield reached their maxima (Figure 3). On the other hand it is shown in Figure 2 that the MPO and MTM solar array temperatures stay above 50°C for the complete period of observation which may explain a higher outgassing from the arrays. Another interesting point is that the MMO solar panels (mounted on the spacecraft side panels) which are completely shielded from the Sun by the MOSIF shield showed a significant temperature and voltage increase (the latter not shown here) for about 4 hr after CA. This may be explained by reflected light from Mercury inside of the MOSIF shield.

There are at least three other interesting details visible from the spectra: (a) The maximum energy of the low energy ions is strictly confined (it is a cold spectrum) but the limit seems different for the three sensors: PICAM sees it at about 70 eV, MIA at about 60 eV and MSA at about 45 eV. None of the sensors has been fully calibrated at these low energies. An analysis of the energy spectra obtained by MIA in the Mercury magnetosphere showed that a downward correction of the energy table at low energies leads to more symmetric Maxwellian spectra (Y. Saito, pers. communication). This would bring the MIA maximum energy closer to the 45 eV observed by MSA. We assume that the differences in maximum energy are an instrumental effect. (b) MSA and MIA total fluxes follow each other closely while the evolution of the flux observed by PICAM is rather different (see Figure 3, “TotalFlux”). (c) Two separate energy bands are observed by all three sensors one at about 40 eV and the other (broader) at 20 eV (for MSA).

It became rather clear from this initial analysis that we observed an effect that has nothing to do with the planetary or solar wind environment but that was caused by outgassing of material from the spacecraft—becoming ionized

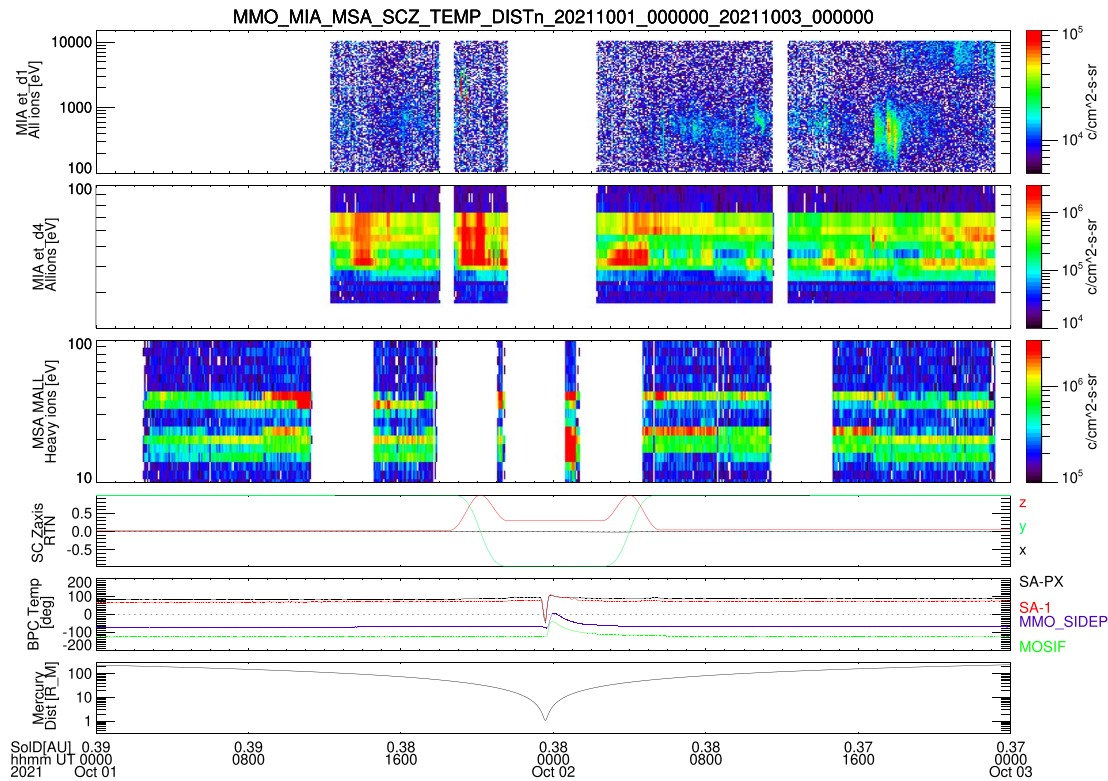


Figure 2. Initial observations by the ion spectrometers onboard MMO for 48hr around the first Mercury flyby. From top to bottom: (1) MIA et-d1 all ion flux spectrum above 100 eV; (2) MIA et-d4 all ion flux spectrum below 100 eV; (3) MSA M3L heavy ion flux spectrum between 10 and 100 eV; (4) Orientation of MMO Z-axis in solar RTN coordinates (Fränz & Harper, 2002); (5) Temperatures on BepiColombo: MPO SolarArray + X (black), MTM SolarArray 1 (red), MMO SidePanel (blue), MOSIF (green); (6) Distance from Mercury in planet radii. “SolDist.” = Solar Distance in AU.

and returning to the spacecraft. Nevertheless, such an intense form of ionized outgassing has not been reported before by any mission. Similar cold low energy ion energy spectra are typical either for planetary ionospheres (e.g., at Mars, Fowler et al., 2022) or when crossing cometary outgassing (Nilsson et al., 2015). In both cases ion densities around the spacecraft are larger than $10^4/\text{cm}^3$. In the following sections we will look at the composition and the dependence on magnetic field and electron fluxes of the signal.

4. Ion Mass Composition

Figure 5 shows the time-of-flight (TOF) distribution observed by the BepiColombo MPPE MSA sensor during the time of the most intense outgassing after Mercury flyby 1 in October 2021. Data from the “TSTL” product were recorded with a time resolution of 256 s. The upper panel compares the TOF spectra observed for the two energy bands. It shows that both energy bands have the same ion mass composition. The lower panel shows a comparison of the observed TOF spectrum with TOF distributions for different ions obtained by an instrument response simulation for MSA (Christophe Verdeil, pers. communication). Unfortunately no simulation for water ions were so far done for the MSA sensor. To be observed molecules have to pass through a thin carbon foil to create a start signal before reaching the MCP which records the stop signal (Delcourt et al., 2016). It is expected that a majority of molecules are broken into their atomic constituents when passing the start carbon foil (Allegrini et al., 2016). The energy loss of molecules in the foil can be estimated by the sum of the energy losses of the atomic constituents (Bragg’s rule, Thwaites (1992)). A major part of constituents leaves the foil neutralized such that no post-acceleration influences the TOF and they should all arrive with a TOF corresponding to mass of the molecule. The observed count ratio between the TOF peaks at mass 1–2 and the peaks at higher masses in Figure 5 is about 0.8. If water molecules would break completely at the top atomic layer of the start foil one would expect a count ratio of 2.0. This means that either only a minor part of water molecules breaks when passing the foil or that there are other ion species in the observed flux. The heavy ion TOF distribution shown in Figure 5 (lower panel, black line) is peaking for the neutralized part at a TOF of 550–600 ns, which suggests a

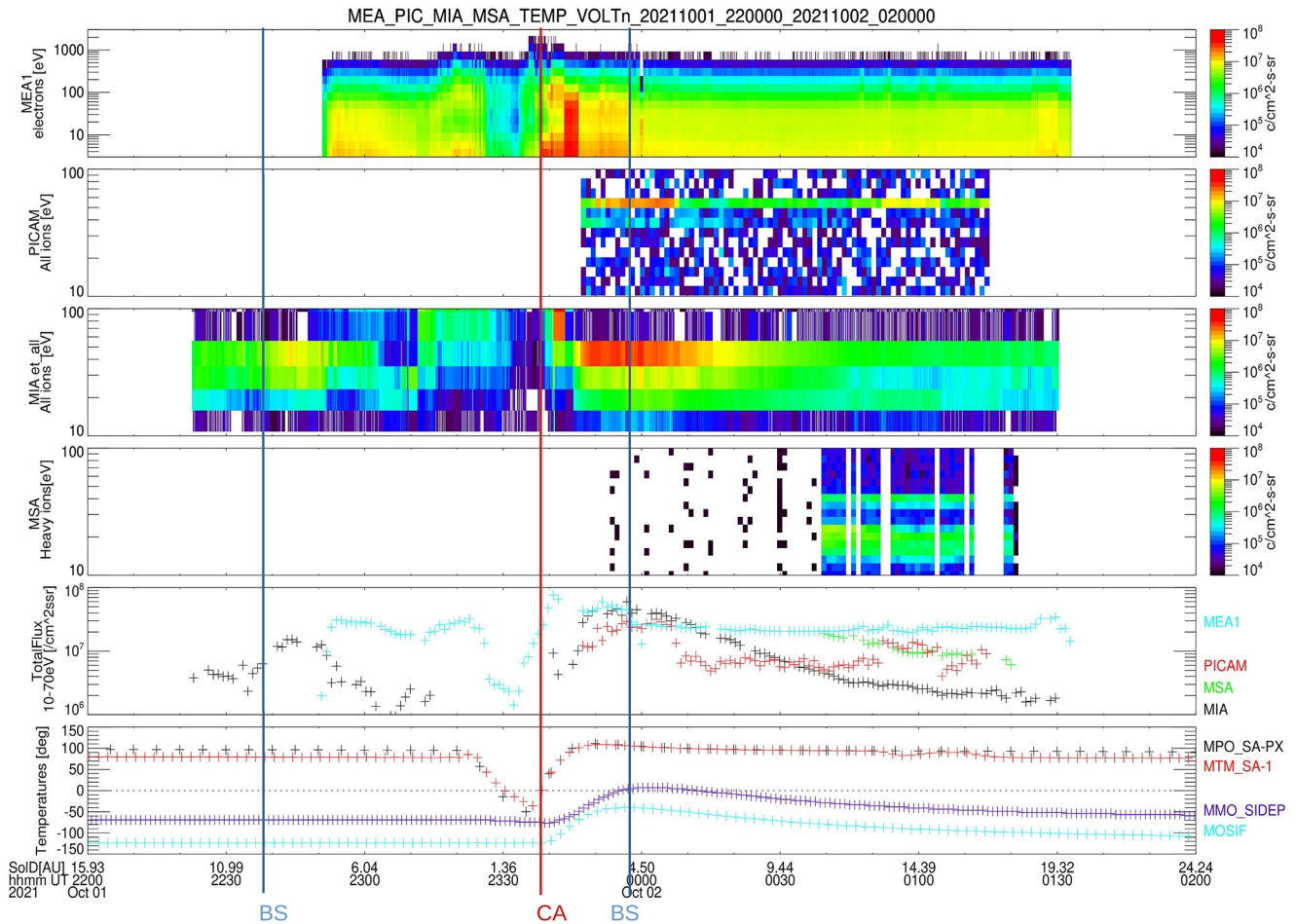


Figure 3. Observations by electron and ion spectrometers for 4 hr around closest approach during the first Mercury flyby. From top to bottom: (1) MEA1 electron flux spectrum above 3 eV; (2) Planetary Ion Camera (PICAM) IMG all ion flux spectrum below 100 eV; (3) MIA et-all all ion flux spectrum below 100 eV; (4) MSA M3L heavy ion flux spectrum between 10 and 100 eV; (5) integrated ion flux 10–70 eV observed by MIA (black), MSA (green), PICAM (red) and electron flux MEA1 (cyan); (6) Temperatures on BepiColombo: MPO SolarArray + X (black), MTM SolarArray Panel 1 (red), MMO SidePanel (blue), MOSIF (cyan); BS = nominal bow shock crossings.

mass of 18–20 amu for the molecules. The respective ionized peak is at TOF 400–450 ns. Since no experimental data are available for the passage of water ions through carbon foils the TOF spectra could possibly be confirmed by simulation. On the other hand Schläppi et al. (2010) observed a high intensity of fluorine (19 amu) in outgassing from Rosetta. We can currently not exclude that atomic fluorine may also be present in the BepiColombo outgassing but it seems that heavier molecules (N_2 , CO_2) are not observed.

5. Influence of Electron Flux and Magnetic Field

Figure 6 shows the ionized outgassing flux in comparison to the observed electron flux and magnetic field orientation for the outbound pass of the first Mercury flyby. The electron flux is measured by the MEA sensors for this period in the energy range 3–2,700 eV. One should note that this excludes most of the photo electron flux toward and from the spacecraft which has typically less than 3 eV energy—specifically if the spacecraft is negatively charged. But the MEA sensors seem to observe a bimodal distribution with an energetic electron peak in the range 30–90 eV (*solar wind electrons*) and another population with energies below 10 eV which we here call *secondary electrons*. The panel marked “TotalFlux Ions <70 eV” shows the total observed ion flux <70 eV for MIA and MSA. MIA shows a much stronger flux variation. This also becomes evident in the flux ratio between lower and upper energy band shown in the next panel. For MIA the lower band vanishes for several hours sometimes while it is persistent in MSA observations. The panels below show the total electron flux and the ratio between secondary and solar wind electron flux. We note that if secondary electron flux increases the lower ion band

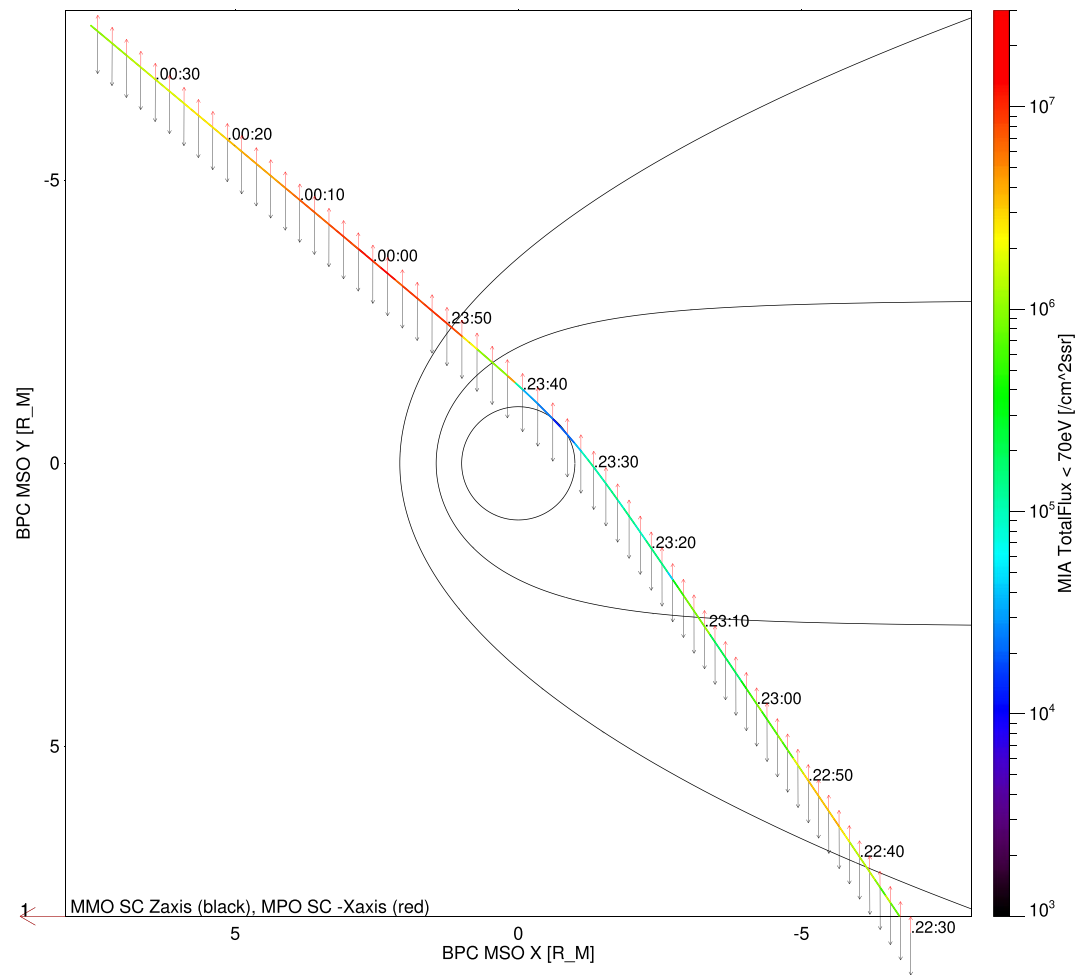


Figure 4. BepiColombo trajectory during first Mercury flyby projected onto the MSO XY coordinate plane. Over-plotted are the MIA total ion flux (10–70 eV) in color and the orientation of the MMO SC Z-axis (black arrows, look direction of MMO sensors) and the MPO -X-axis (red arrows, look direction of Planetary Ion Camera). Additional lines show the non-aberrated bow shock and magnetopause locations (Winslow et al., 2013). Time tags are in UTC along the trajectory for the period 1 October 2021 22:30 to 2 October 2023 00:30 UTC.

appears in MIA observations and the respective total ion flux increases as well. The two bottom panels show the magnetic field observed by the MGF sensor onboard MMO: total field magnitude and polar and azimuth angles in MMO spacecraft coordinates (see. Figure 1) where “theta” is the angle with the Z-axis and “phi” is counted from the positive X-axis. We note that these angles do not change very much except for two periods on 2 October, 05:00–08:00 UTC and 17:00–18:00 UTC. In the first case this is coincident with increased secondary electron fluxes and increased lower band ion fluxes observed by MSA. It may be important that the theta angle has almost always values larger than 120° during this period. That means that the field is more parallel to the spacecraft Z-axis. This could lead to an increased current inside of the MOSIF shield.

It was realized after analyzing these first Mercury flyby observations that the spacecraft encountered an unusual plasma physical phenomenon. For this reason a special campaign was planned for March 2022 where all spectrometers were switched on for three consecutive days in low energy mode. Also the magnetometers were switched on for this campaign.

Figure 7 shows respective data obtained between 11 and 15 March 2022, when BepiColombo was in pure solar wind at solar distances between 0.43 and 0.46 AU. The top panel shows energetic ion spectra observed by MIA. One can see that there was a solar energetic particle event starting on March 11 around 16:00 UTC and ending on March 12 around 12:00 UTC. This event also caused an increase in low energy ionized outgassing shown in the three panels below. We may assume that the energetic particle impact probably did not increase the neutral

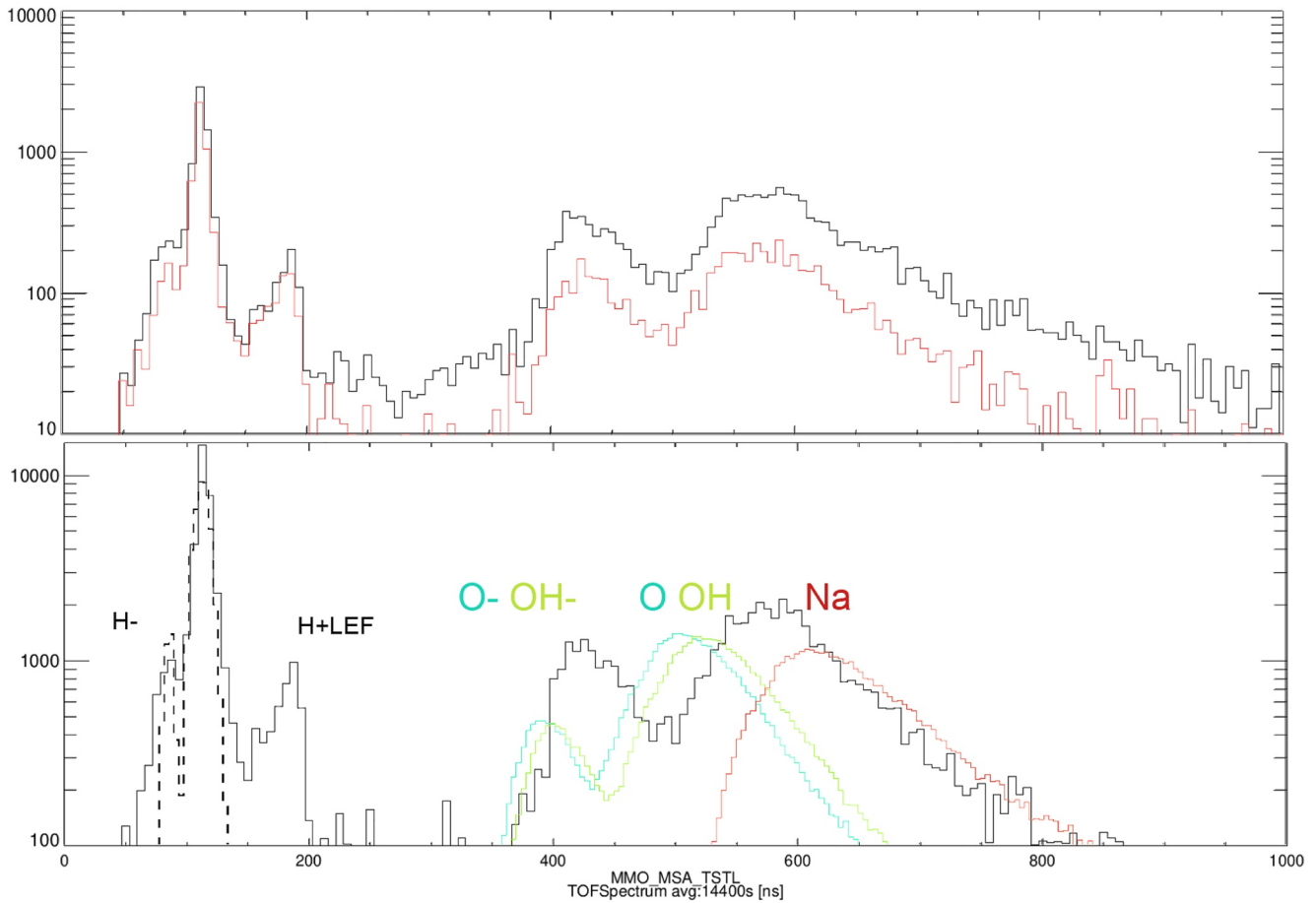


Figure 5. Time-of-flight spectra observed by the BepiColombo MSA sensor accumulated over 4 hr in solar wind on the Mercury Flyby-1 outbound pass 2 October 2021 08:00–12:00 UTC. The X-axis denotes ion time-of-flight in ns, the vertical axis accumulated counts. The upper panel shows accumulated counts in the 10–30 eV energy band (black) and the 30–50 eV energy band (red). The lower panel shows total accumulated counts 10–50 eV (black solid) and simulated response curves for different incoming ion species: H+ (black dashed), O+ (blue), OH+ (green), Na+ (red). Incoming ions arrive either as neutrals or negatively charged at the MSA Stop anode resulting in a split TOF distribution. The peak marked as “H + LEF” is caused by protons hitting the upper LEF anode of MSA causing secondary electron emission.

outgassing but the ionization frequency. What is immediately obvious from the three low energy ion panels is that the intensity of the signal is much weaker than during observations during the first Mercury flyby. The lower band appears only on March 14 00:00–12:00 UTC. The cut-off energy is around 25 eV but varies. For this reason the PICAM sensor was not able to see the signal at all (not shown here). The panel marked “MEA1 electrons” shows electron spectra obtained by MEA1. The sensor operated in solar wind mode with low-energy table ranging from 3 to 280 eV. We observe again a bimodal distribution with solar wind electrons above ≈ 17 eV and secondary electrons below ≈ 17 eV. The ratio between the secondary electron and solar wind electron flux is shown in a separate panel. We also show the variation of the magnetic field obtained by the MGF instrument in the same coordinates as in Figure 6. We can see that shorter increases of the low energy ion flux on 13 March and 14 March coincide with changes in the magnetic field orientation—though not all major changes in the field orientation result in an ion flux increase. We also note that the theta angle is close to 90° most of the time in this period. This means the electron current into the MOSIF shield may be reduced compared to the Mercury flyby period—though this is not visible in the observed part of the electron spectrum.

Another important correlation becomes visible through the two bottom panels showing the temperatures and attitude of the solar arrays. The black line marked “MTM-SA-Z-th” shows the angle between the large MTM solar arrays surface normal and the solar direction. One can see that this angle is around 101 deg but has regular variations by 1–2 deg every 24 hr. These changes coincide with the regular rotation around the spacecraft central axis happening every 12 hr. This has no major impact on the total illumination of the spacecraft. But the small

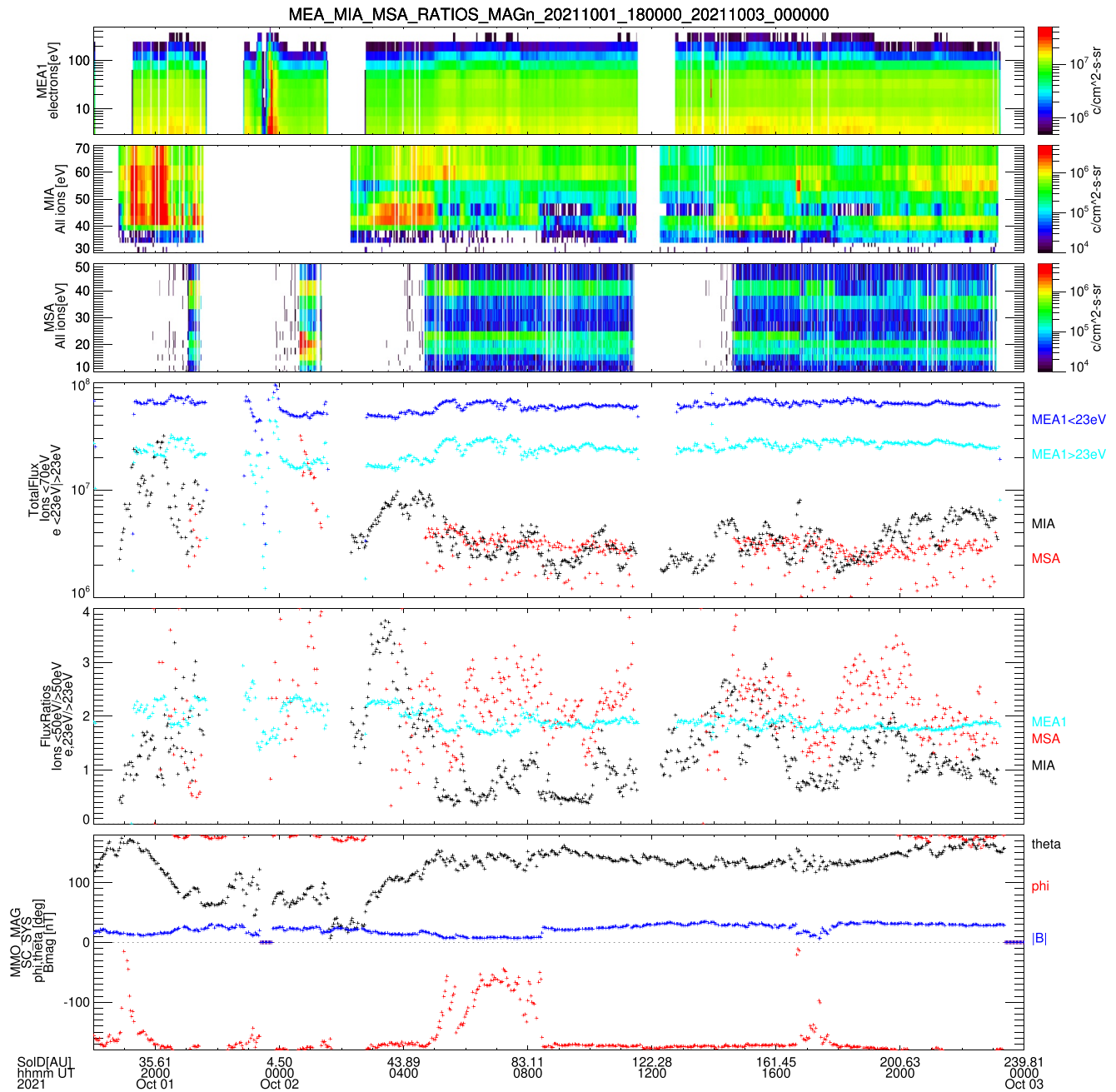


Figure 6. Electron, ion and magnetic field observations around the first Mercury flyby, from top to bottom: (1) MEA1 electron flux spectrum; (2) MIA et-d4 ion flux spectrum (30–70 eV); (3) MSA Mall ion flux spectrum (10–50 eV); (4) Total fluxes [cm^2ssr] ions <70 eV MIA (black), MSA (red); electrons >23 eV (blue) MEA1 (5) flux ratios electrons <23 eV/ >23 eV MEA1 (cyan); ions MIA <50 eV/ >50 eV (black), MSA <30 eV/ >30 eV (red) (6) MMO MGF magnetic field angles in MMO spacecraft coordinates azimuth (ϕ —red), polar (θ —black) and total field [nT] (blue).

changes in the solar array attitude have strong correlation to the array temperatures shown in the panel above. These variations in array attitude seem to influence the cut-off energy of the outgassing ions shown in panel “MSA All ions” and the electron fluxes. This cut-off energy represents the negative spacecraft potential.

6. Evolution With Solar Distance and Time

If we now plot daily averages of the total ion flux ≤ 50 eV observed by the MSA sensor as a function of time (Figure 8) we first observe a large variation of fluxes during each measurement interval. But also we see between

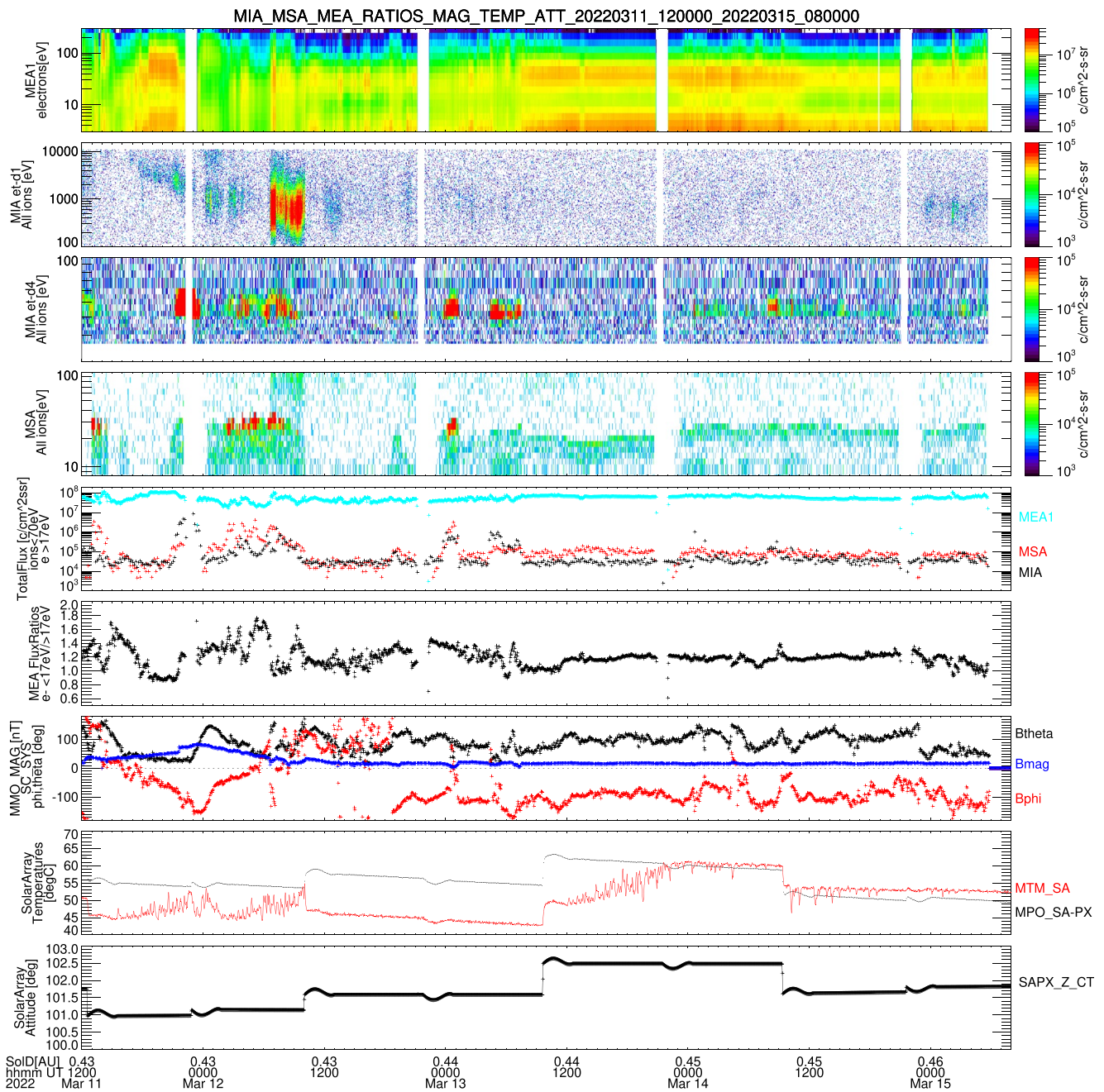


Figure 7. Electron, ion and magnetic field observations in solar wind cruise of March 2022, from top to bottom: (1) MEA1 electron flux spectrum; (2) MIA et-d1 ion flux spectrum (100–15,000 eV); (3) MIA et-d4 ion flux spectrum (15–100 eV); (4) MSA all ion flux spectrum (1–50 eV); (5) Total fluxes [$1/\text{cm}^2\text{ssr}$] ions <70 eV MIA (black), MSA (red), electrons >17 eV (cyan); (6) electron flux ratios $(3\text{--}17\text{ eV})/(17\text{--}100\text{ eV})$ MEA1; (7) MMO MGF magnetic field angles in MMO spacecraft coordinates azimuth (ϕ —red), polar (θ —black); magnitude [nT] (blue); (8) Temperatures [$^{\circ}\text{C}$] of solar arrays on MPO (black), MTM (red); (9) Angle of MTM solar array normal axis with the solar direction (black). All data are time averaged over 128 s.

the first Mercury flyby (“MFB1”) and end 2022 an exponential decrease of the ion flux maxima with a time constant of about 100 days. But during the 3rd flyby (“MFB3”) in June 2023 fluxes increased again which is confirmed by the latest measurement in cruise in October 2023. The lower panel of Figure 8 shows the distance of BepiColombo from Sun, Mercury and Venus.

In Figure 9 we plot spacecraft temperatures and ionized outgassing flux as function of solar distance. The plot covers available temperature and flux data in cruise and during 2 Venus and 2 Mercury flybys. The top panel shows temperature data of the MOSIF shield, the MMO side panels, the MTM body and the solar arrays. The

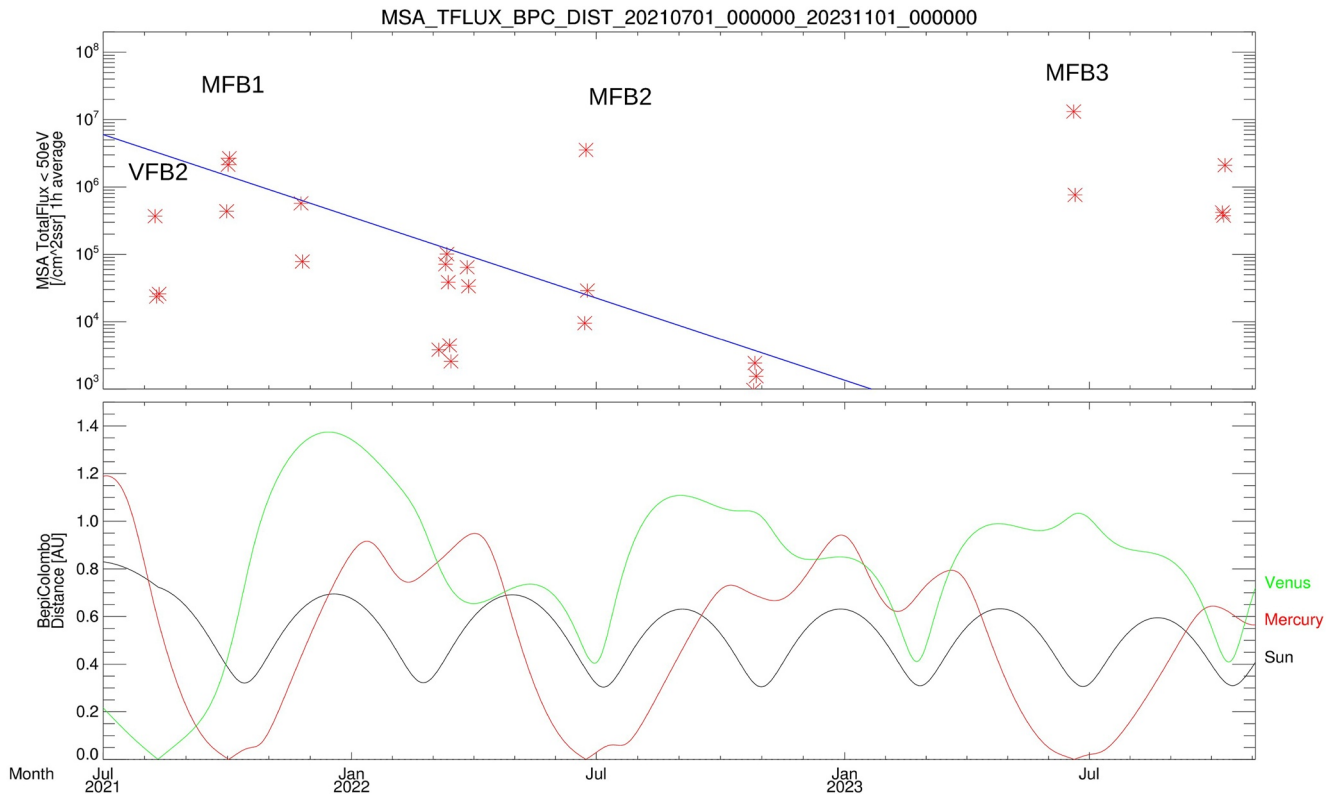


Figure 8. Evolution of BepiColombo outgassing as function of time for the BepiColombo cruise phase and flybys in daily averages up to November 2023. The blue line indicates an exponential decrease with a time constant of 100 days. (Top) MSA Mall total ion flux (10–50 eV). (Bottom) Distance [AU] of BepiColombo from Sun (black), Mercury (red), Venus (green).

MMO and MOSIF stay below -70°C except for the flybys at 0.36 and 0.72 AU where they can rise up to 0°C . The MTM body can reach temperatures up to 20°C during Mercury flyby. The solar arrays are always above this temperature and can reach up to 100°C . The bottom panel shows daily averages of ion fluxes below 70 eV observed by the MIA and MSA sensors. Background counts covering the whole energy spectrum have been removed before taking the daily averages. The black lines indicate exponential fall offs with distance $d[\text{AU}]$ with a scale height of $1/7$ for temperature and $2/7$ for the ionized outgassing. One can see that while temperature follows the exponential except for the closest approaches to the planets. This is presumably caused by the planetary heat reflection. Ionized outgassing seems to follow the exponential only outside 0.5 AU. Within this distance either the outgassing increases or the ionization.

7. Interpretation

Before discussing possible explanations let us summarize the observations:

1. BepiColombo observed low energy ion spectra with a sharp upper cut-off through most phases of the cruise phase in 2021 and 2022 (Figures 2 and 7).
2. Outside 0.5 AU distance from the Sun ionized fluxes are approximately proportional to the square root of temperature, inside of 0.5 AU they show a stronger increase. This is indicated by the ratio of the exponential fall-offs with distance shown by the black lines in Figure 9.
3. The upper cut-off energy seems to be correlated to the attitude of the solar arrays (Figure 7).
4. The ion composition indicates that we mainly observe ionized water molecules (though fluorine can not be excluded, Figure 5).
5. At the first Mercury flyby the cut-off energy was highest and two separate energy bands at 20 and 45 eV (MSA calibration) were observed by MSA, MIA, and PICAM (Figure 3).
6. The intensity of the lower band (observed by MIA) varies with the secondary electron flux <20 eV (Figure 6).

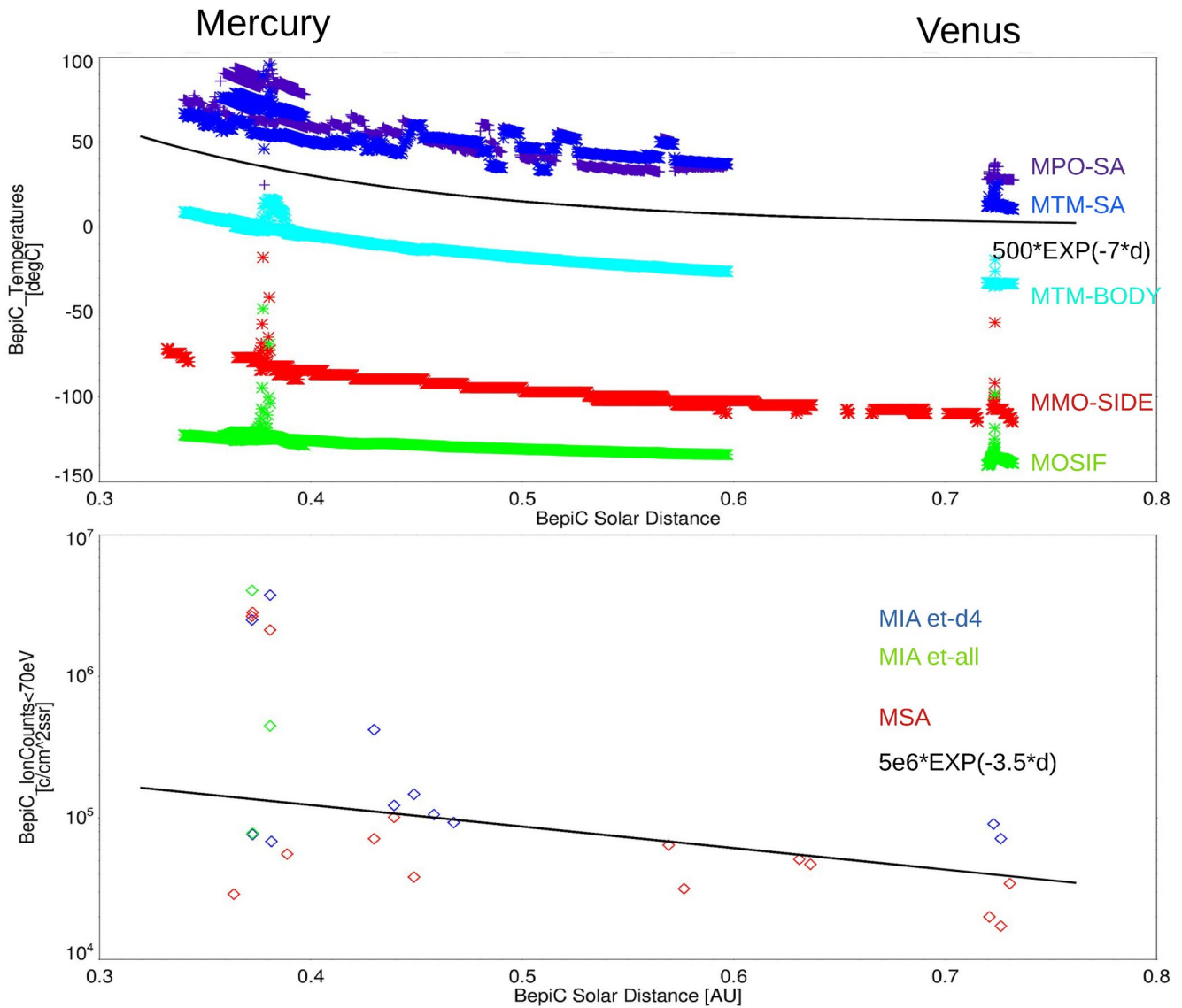


Figure 9. Evolution of BepiColombo temperatures (top) and ionized outgassing (bottom) as a function of solar distance for the BepiColombo cruise phase and flybys up to July 2022. (Top) Temperatures [°C] of solar arrays, MTM body, MMO side panel and MOSIF shield, hourly averages. (Bottom) (1) MIA et-d4 and et-all total ion flux (20–70 eV); (2) MSA total ion flux (10–50 eV), daily averages. The black lines indicate exponential fall offs with distance.

7. The short time variation of the intensity is influenced by the total electron flux and the local magnetic field orientation (Figures 6 and 7).
8. The total solar wind electron flux during the first Mercury flyby is on the order of about $3 \times 10^7/\text{cm}^2\text{ssr}$ corresponding to an omni-directional flux of $F_e \approx 4 \times 10^8/\text{cm}^2\text{s}$, the observed low energy ion flux is about $F_i = 3 \times 10^6/\text{cm}^2\text{ssr}$ (Figure 6).

It is clear that these observations indicate an effect caused by outgassing from the spacecraft—probably dominated by water sublimation. A sketch of the general situation is shown in Figure 10. It is also clear that the sharp upper cut-off energy must be caused by acceleration of the ions by a spacecraft potential. It is in principle possible that since different parts of the BepiColombo spacecraft surfaces in stacked configuration are made of dielectrics and conductive materials, these surfaces can charge up to different voltages. To our knowledge high surface conductivity was only implemented for the MPO and MMO satellites as separate units. This means that at least the spacecraft potential for MIA, MEA, and MSA is the same such that the apparent differences of the cut-off energy between MIA and MSA must be caused by different instrument calibrations.

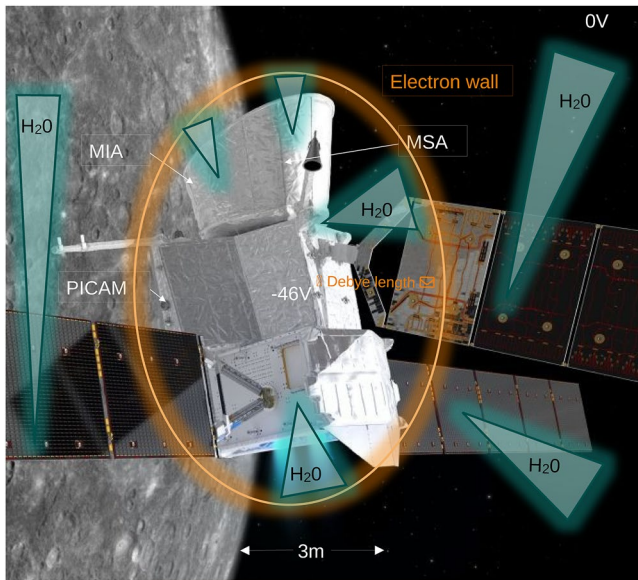


Figure 10. Sketch of the physical situation of the BepiColombo spacecraft during Mercury flyby based on an artistic drawing (Copyright:ESA). The spacecraft central Z-axis is perpendicular to the solar direction which is parallel to the positive X-axis. The MPO solar array is aligned in the X-Z plane such that the array is hardly illuminated. The MTM solar array attitude is not shown correctly. They are at a flat angle (11 deg) with the solar direction. Shown is also the position of Planetary Ion Camera on MPO and the position of MIA and MSA inside of the MOSIF shield. The green triangles indicate possible locations of outgassing. The orange ellipse indicates the Debye sphere forming around the spacecraft by repelling of cold electrons by the negative spacecraft potential of -46 V.

In a typical thin solar wind plasma close to Earth spacecraft usually charge up to a small positive potential but it was predicted by Ergun et al. (2010) that in a high electron flux environment closer to the Sun spacecraft should charge to high negative potentials (up to -80 V) when the local Debye length is smaller than the spacecraft dimensions. The **Debye length** in a cold plasma is given by $\lambda_D = \sqrt{\frac{\epsilon_0 k_B T_e}{n_e q_e^2}}$ and defines the mean free path of electrons. From observations by the PICAM sensor (Orsini et al., 2022) we know that during the first Mercury flyby solar wind velocity was around 340 km/s. No calibrated density measurement was possible but a plasma density value of $100/\text{cm}^3$ is typical for 0.3 AU. This would also agree with the solar wind electron flux observed by MEA—though MEA observes only perpendicular to the solar wind. With an electron temperature of about 10^5 K we can assume a Debye length on the order of meters as indicated in Figure 10. If the local plasma density is increased by ionized outgassing the Debye length may become even shorter. In this case the plasma environment may be compared to inside cometary plumes as observed by the Rosetta spacecraft (Johansson et al., 2021) where a spacecraft potential of -45 V indicated a local electron density of $>10^4/\text{cm}^3$. But we note, that cometary plumes contain a much colder plasma compared to the BepiColombo case such that the effect of the solar electron flux on the potential will probably dominate.

At first Mercury flyby the observed ion flux was $F_i = 3 \times 10^6/\text{cm}^2\text{ssr}$, at a medium energy of 30 eV the water ion velocity is about $v_i = 18$ km/s. This corresponds to a water ion density of about $n_i = F_i/v_i = 1.7/\text{cm}^3$. This means that the local plasma density is not significantly increased by the ionized water density at the point of observation. It also means that the effect of the outgassing on the spacecraft potential is probably minor. To estimate the corresponding neutral water density we need to consider photo ionization and electron impact ionization. The photo ionization frequency of water molecules in solar radiation is rather well known, Huebner and Mukherjee (2015)

give a value of 8.3×10^{-7} Hz for the active Sun at Earth orbit. The solar distance at first Mercury flyby was 0.38 AU such that we should expect a photo ionization frequency seven times higher: $f_{ph} = 5.8 \times 10^{-6}$ Hz. The dissociation of water molecules has a 20 times higher frequency (Huebner & Mukherjee, 2015) but multiplied with the subsequent ionization frequencies it plays a minor role.

Electron ionization cross section for water molecules are reviewed by Song et al. (2021). They report a flat spectrum between 20 and 300 eV peaking at 100 eV electron energy with a value of $\sigma_e = 2 \times 10^{-16}$ cm^2 . With the observed electron flux this would result in an electron impact ionization frequency of: $f_e = F_e \times \sigma_e = 8 \times 10^{-8}$ Hz which is almost two orders lower than the photo ionization frequency. Taking these frequencies and the observed ion density n_i we arrive at a neutral water density of $n_w = n_i/(f_{ph} + f_e) = 2.8 \times 10^5/\text{cm}^3$. Of course all these numbers depend on very preliminary calibration of the instruments but the order of magnitude should be correct. This estimate agrees also very well with the water vapor density of $5 \cdot 10^5/\text{cm}^3$ estimated for the Rosetta spacecraft outgassing by Schläppi et al. (2010). This also implies that a similar calculation of the total water loss from the spacecraft can be based on the back scattering formula by Robertson (1976). This means that the loss of mass by outgassing from the BepiColombo is comparable to the value derived by Schläppi et al. (2010) for the Rosetta spacecraft (about 2 kg/ m^2yr).

From a perspective of plasma physics the most interesting feature of the observations is the double-band structure of the energy spectra. In the following we discuss different thoughts to explain this observation:

- (a) One can first think that we see in these bands ions with same energy but different charge states since the ion spectrometers filter by energy per charge and not by total energy. But first the probability of double charging water molecules is very low and would lead to a much lower intensity of the lower band. Second an electro-static spacecraft potential will accelerate a double charged ion also to double energy such that they will arrive at the sensor also with double energy. One would need a rather specific setup where ions double charge only within the Debye sphere and thus get a lower energy to support this explanation.

- (b) One proposed idea was that the spacecraft does not charge up negatively but the 3 solar arrays charge to different positive voltages (Stas Barabash, pers. communication). Then water molecules ionized very close to the solar arrays would be repelled from the arrays and arrive with respective different energies. With respect to the high observed electron currents a positive charging is improbable—though this must be confirmed by simulation of the solar array surfaces. Also this would mean conductivity between spacecraft and solar arrays is very low. Finally one can easily prove by simulation or analytically that no significant ion flux can return to inside the MOSIF shield in this setup. For these reasons we can rule out this explanation.
- (c) As predicted by Ergun et al. (2010) and Guillemant et al. (2013) the dimension of the Debye length is crucial for the potential of the spacecraft and the shape of the potential around the spacecraft. Since part of the electron spectrum is repelled by the negative potential of the spacecraft one can think of a sphere of Debye radius around the spacecraft beyond which the electron spectrum changes. Only outside of this sphere the potential will fall off exponentially—probably with a scale height of the Debye length. The actual potential distribution around the spacecraft can be by far more complicated. As the analysis by Guillemant et al. (2013) shows one needs a Debye length on decimeter scales to explain a spacecraft potential of -45 V. This means that not the solar wind electrons but secondary electrons must dominate the BepiColombo space environment and would also explain the observed bimodal electron spectrum. If there are now water sublimation sources with different pressures on the spacecraft they will form gas plumes with different density scale heights. Water ionized outside of the Debye sphere will be accelerated to the full spacecraft potential, water ionized inside of the Debye sphere will encounter a respectively lower potential. A modification of this picture can be that water ionized in the shadowed regions or the plasma wake of the spacecraft encounters a different potential relative to the spacecraft. We also investigated at which distances the water ion sources must be located to match the observed two-band energy spectrum using a particle-in-cell (PIC) simulation using the Starfish PIC code developed by Lubas Brieda (Brieda, 2018). The simulation results showed that ion sources located at about 3 and 6 m distance from the point of observation can replicate the observed two-band flux spectrum.

8. Conclusions

During the first Mercury flyby of BepiColombo the 3 ion spectrometers MPPE-MIA, MPPE-MSA, and SERENA-PICAM observed a strong flux of ions with energies of less than 70 eV. The energy spectra showed a double band structure with a strict upper cut-off. The composition of the ions is dominated by water molecules. Similar signals were observed later during cruise phase at lower energy and intensity and also during the second and third Mercury flybys. The signal is interpreted as being caused by spacecraft outgassing. This is supported by the correlation between signal intensity and spacecraft temperatures. To our knowledge this is the first observation of outgassing observed by ion spectrometers. We interpret the upper cut-off energy as being caused by a negative charging of the spacecraft caused by the strong secondary electron fluxes in agreement with predictions by Guillemant et al. (2013). The highly negative observed potential indicates that the specific geometry of the stacked BepiColombo spacecraft causes a domination of the local plasma by secondary electrons. The electron flux is also identified as the dominant ionization source by the dependence of the fluxes on magnetic field and electron spectra. The double band structure of the energy spectra can be explained by different ion populations originating close to the spacecraft (within a Debye length or inside of a plasma wake) and ion populations generated at larger distance from the spacecraft. A simplified 2D PIC simulation supports this explanation. More sophisticated simulations including the full electron spectra and properties of the spacecraft surfaces are needed to get a complete understanding of the physics.

Data Availability Statement

The raw ion and electron spectrometer data of the MPPE instrument used in this study are publicly available through the AMDA website (AMDA-consortium, 2023). The mentioned PIC code is available at (Brieda, 2023). All other data presented in the time series figures are available as a set through Fränz (2023).

References

- Allegri, F., Ebert, R. W., & Funsten, H. O. (2016). Carbon foils for space plasma instrumentation. *Journal of Geophysical Research (Space Physics)*, *121*(5), 3931–3950. <https://doi.org/10.1002/2016JA022570>
- AMDA-consortium. (2023). BepiColombo MPPE dataset at AMDA, CDPP [Dataset]. Repository. Retrieved from <http://amda.irap.omp.eu/>
- Baumjohann, W., Matsuoka, A., Narita, Y., Magnes, W., Heyner, D., Glassmeier, K. H., et al. (2020). The BepiColombo-Mio Magnetometer en route to Mercury. *Space Science Reviews*, *216*(8), 125. <https://doi.org/10.1007/s11214-020-00754-y>

Acknowledgments

We thank the MPPE, MGF and SERENA instrument teams of the BepiColombo mission for providing excellent calibrated data. We thank the BepiColombo ground operation teams at ESAC, Madrid, and ISAS, Tokyo, for providing spacecraft housekeeping data. We also thank Lubos Brieda for providing the Starfish PIC code. This work was supported by Grant 50QW2101 of German space agency DLR. French co-authors acknowledge the support of CNES for the BepiColombo mission. Open Access funding enabled and organized by Projekt DEAL.

- Benkhoff, J., Murakami, G., Baumjohann, W., Besse, S., Bunce, E., Casale, M., et al. (2021). BepiColombo—Mission overview and science goals. *Space Science Reviews*, 217(8), 90. <https://doi.org/10.1007/s11214-021-00861-4>
- Brieda, L. (2018). Model for steady-state fully kinetic ion beam neutralization studies. *IEEE Transactions on Plasma Science*, 46(3), 556–562. <https://doi.org/10.1109/TPS.2018.2801282>
- Brieda, L. (2023). Starfish particle in cell code [Software]. Repository. Retrieved from <https://www.particleincell.com/starfish/>
- Delcourt, D., Saito, Y., Leblanc, F., Verdeil, C., Yokota, S., Fraenz, M., et al. (2016). The mass spectrum analyzer (MSA) on board the BepiColombo MMO. *Journal of Geophysical Research (Space Physics)*, 121(7), 6749–6761. <https://doi.org/10.1002/2016JA022380>
- Diaz-Aguado, M. F., Bonnell, J. W., Bale, S. D., Wang, J., & Gruntman, M. (2021). Parker solar probe FIELDS instrument charging in the near Sun environment: Part 2: Comparison of in flight data and modeling results. *Journal of Geophysical Research (Space Physics)*, 126(5), e28689. <https://doi.org/10.1029/2020JA028689>
- Ergun, R. E., Malaspina, D. M., Bale, S. D., McFadden, J. P., Larson, D. E., Mozer, F. S., et al. (2010). Spacecraft charging and ion wake formation in the near-Sun environment. *Physics of Plasmas*, 17(7), 072903. <https://doi.org/10.1063/1.3457484>
- Fowler, C. M., McFadden, J., Hanley, K. G., Mitchell, D. L., Curry, S., & Jakosky, B. (2022). In-Situ measurements of ion density in the Martian ionosphere: Underlying structure and variability observed by the MAVEN-STATIC instrument. *Journal of Geophysical Research (Space Physics)*, 127(8), e30352. <https://doi.org/10.1029/2022JA030352>
- Fränz, M. (2023). BepiColombo outgassing study dataset 2023 (original submission) [Dataset]. Zenodo repository. <https://doi.org/10.5281/zenodo.8223967>
- Fränz, M., & Harper, D. (2002). Heliospheric coordinate systems. *Planet. Space Sci.*, 50(2), 217–233. [https://doi.org/10.1016/S0032-0633\(01\)00119-2](https://doi.org/10.1016/S0032-0633(01)00119-2)
- Green, D. B. (2001). Satellite contamination and materials outgassing knowledgebase—An interactive database reference. In *Technical report, NASA/CR-2001-210909; M-1010; NAS 1.26:210909*.
- Guillemant, S., Génot, V., Matéo-Vélez, J. C., Ergun, R., & Louarn, P. (2012). Solar wind plasma interaction with solar probe plus spacecraft. *Annales Geophysicae*, 30(7), 1075–1092. <https://doi.org/10.5194/angeo-30-1075-2012>
- Guillemant, S., Genot, V., Velez, J.-C. M., Sarrailh, P., Hilgers, A., & Louarn, P. (2013). Simulation study of spacecraft electrostatic sheath changes with the heliocentric distances from 0.044 to 1 AU. *IEEE Transactions on Plasma Science*, 41(12), 3338–3348. <https://doi.org/10.1109/TPS.2013.2246193>
- Hadid, L. Z., Génot, V., Aizawa, S., Milillo, A., Zender, J., Murakami, G., et al. (2021). BepiColombo's cruise phase: Unique opportunity for synergistic observations. *Frontiers in Astronomy and Space Sciences*, 8, 154. <https://doi.org/10.3389/fspas.2021.718024>
- Huebner, W. F., & Mukherjee, J. (2015). Photoionization and photodissociation rates in solar and blackbody radiation fields. *Planetary and Space Science*, 106, 11–45. <https://doi.org/10.1016/j.pss.2014.11.022>
- Isensee, U., & Maassberg, H. (1981). Particle-in-cell simulation of the plasma environment of a spacecraft in the solar wind. *Advances in Space Research*, 1(2), 413–416. [https://doi.org/10.1016/0273-1177\(81\)90315-X](https://doi.org/10.1016/0273-1177(81)90315-X)
- Johansson, F. L., Eriksson, A. I., Gilet, N., Henri, P., Wattiaux, G., Taylor, M. G. T., et al. (2020). A charging model for the Rosetta spacecraft. *A&A*, 642, A43. <https://doi.org/10.1051/0004-6361/202038592>
- Johansson, F. L., Eriksson, A. I., Vigren, E., Bucciantini, L., Henri, P., Nilsson, H., et al. (2021). Plasma densities, flow, and solar EUV flux at comet 67P. A cross-calibration approach. *A&A*, 653, A128. <https://doi.org/10.1051/0004-6361/202039959>
- Mangano, V., Dósa, M., Fränz, M., Milillo, A., Oliveira, J. S., Lee, Y. J., et al. (2021). BepiColombo science investigations during cruise and flybys at the Earth, Venus and Mercury. *Space Science Reviews*, 217(1), 23. <https://doi.org/10.1007/s11214-021-00797-9>
- Murad, E. (1985). Implications of mass spectrometric measurements on space shuttle. *Planetary and Space Science*, 33(4), 421–423. [https://doi.org/10.1016/0032-0633\(85\)90087-X](https://doi.org/10.1016/0032-0633(85)90087-X)
- Murakami, G., Hayakawa, H., Ogawa, H., Matsuda, S., Seki, T., Kasaba, Y., et al. (2020). Mio—First comprehensive exploration of Mercury's space environment: Mission overview. *Space Science Reviews*, 216(7), 113. <https://doi.org/10.1007/s11214-020-00733-3>
- Nilsson, H., Stenberg Wieser, G., Behar, E., Simon Wedlund, C., Gunell, H., Yamauchi, M., et al. (2015). Birth of a comet magnetosphere: A spring of water ions. *Science*, 347(6220), aao571. <https://doi.org/10.1126/science.aao571>
- Odelstad, E., Eriksson, A. I., Edberg, N. J. T., Johansson, F., Vigren, E., André, M., et al. (2015). Evolution of the plasma environment of comet 67P from spacecraft potential measurements by the Rosetta Langmuir probe instrument. *Geophysical Research Letters*, 42(23), 10126–10134. <https://doi.org/10.1002/2015GL066599>
- Odelstad, E., Stenberg-Wieser, G., Wieser, M., Eriksson, A. I., Nilsson, H., & Johansson, F. L. (2017). Measurements of the electrostatic potential of Rosetta at comet 67P. *MNRAS*, 469(Suppl_2), S568–S581. <https://doi.org/10.1093/mnras/stx2232>
- Orsini, S., Livi, S. A., Lichtenegger, H., Barabash, S., Milillo, A., & Angelis, E., et al. (2021). SERENA: Particle instrument suite for determining the Sun-Mercury interaction from BepiColombo. *Space Science Reviews*, 217(1), 11. <https://doi.org/10.1007/s11214-020-00787-3>
- Orsini, S., Milillo, A., Lichtenegger, H., Varsani, A., Barabash, S., Livi, S., et al. (2022). Inner southern magnetosphere observation of Mercury via SERENA ion sensors in BepiColombo mission. *Nature Communications*, 13(1), 7390. <https://doi.org/10.1038/s41467-022-34988-x>
- Robertson, S. (1976). Spacecraft self-contamination due to back-scattering of outgas products. In *Interim report LMSC-HREC TR D496676*. Lockheed Missions and Space Co.
- Saito, Y., Delcourt, D., Hirahara, M., Barabash, S., André, N., Takashima, T., et al. (2021). Pre-flight calibration and near-Earth commissioning results of the Mercury plasma particle experiment (MPPE) onboard MMO (Mio). *Space Science Reviews*, 217(5), 70. <https://doi.org/10.1007/s11214-021-00839-2>
- Schirmer, M., Schirmer, M., Thürmer, K., Bras, B. E. A., Martin-Fleitas, J., Goueffon, Y., et al. (2023). Euclid preparation. XXIX. Water ice in spacecraft Part I: The physics of ice formation and contamination. *A&A*, 675, A142. <https://doi.org/10.1051/0004-6361/202346635>
- Schläppi, B., Altwegg, K., Balsiger, H., Hässig, M., Jäckel, A., Wurz, P., et al. (2010). Influence of spacecraft outgassing on the exploration of tenuous atmospheres with in situ mass spectrometry. *Journal of Geophysical Research (Space Physics)*, 115(A12), A12313. <https://doi.org/10.1029/2010JA015734>
- Song, M.-Y., Cho, H., Karwasz, G. P., Kokouline, V., Nakamura, Y., Tennyson, J., et al. (2021). Cross sections for electron collisions with H₂O. *Journal of Physical and Chemical Reference Data*, 50(2), 023103. <https://doi.org/10.1063/5.0035315>
- Thwaites, D. I. (1992). Departures from Bragg's rule of stopping power additivity for ions in dosimetric and related materials. *Nuclear Instruments and Methods in Physics Research B*, 69(1), 53–63. [https://doi.org/10.1016/0168-583X\(92\)95738-D](https://doi.org/10.1016/0168-583X(92)95738-D)
- Uy, O. M., Green, B. D., Wood, B. E., Galica, G. E., Boies, M. T., Lesho, J. C., et al. (2003). The gaseous and particle environment observed above the MSX spacecraft after seven years on orbit. In K. Fletcher (Ed.), *Materials in a space environment* (Vol. 540, pp. 197–202).

- Voigt, G. H., Isensee, U., & Haassberg, H. (1981). The interactions of the HELIOS probe with the solar wind plasma. In *Final report, Mar. 1981 Technische Hochschule, Darmstadt (Germany, F.R.)*. Angewandte Geophysik.
- Winslow, R. M., Anderson, B. J., Johnson, C. L., Slavin, J. A., Korth, H., Purucker, M. E., et al. (2013). Mercury's magnetopause and bow shock from MESSENGER Magnetometer observations. *Journal of Geophysical Research (Space Physics)*, *118*(5), 2213–2227. <https://doi.org/10.1002/jgra.50237>